JOURNAL OF PHYSICAL ORGANIC CHEMISTRY
J. Phys. Org. Chem. 2006; **19:** 540–551
Published online 21 June 2006 in Wiley InterScience (www.interscience.wiley.com). DOI: 10.1002/poc.1053

IR spectroscopic strategies for the structural characterization of isolated and microsolvated arenium ions†

Otto Dopfer*

Institut für Atomare Physik und Fachdidaktik, Technische Universität Berlin, Hardenbergstrasse 36, D-10623 Berlin, Germany

Received 2 November 2005; revised 6 December 2005; accepted 7 December 2005

ABSTRACT: This contribution summarizes recent experimental developments in coupling modern sensitive IR spectroscopic techniques with selective mass spectrometric methods, which have allowed for the first time for the unambiguous structural characterization of isolated and microsolvated protonated aromatic molecules in the gas phase. The two major experimental strategies involve (i) single-photon IR photodissociation (IRPD) spectroscopy in a tandem quadrupole mass spectrometer using novel optical parametric oscillator (OPO) laser systems in the 2500–4000 cm^{-1} range and (ii) IR multiphoton dissociation (IRMPD) spectroscopy in a Fourier transform ion cyclotron resonance (FT-ICR) mass spectrometer using high-intensity free electron lasers (FEL) in the 500–2500 cm^{-1} range. Both techniques offer complementary spectroscopic information, which is highlighted for the various isomers of protonated fluorobenzene, a simple prototype for protonated aromatic molecules. The analysis of the IR spectra provides unprecedented experimental insight into structure, energetics, and chemical reactivity of these fundamental reactive intermediates under isolated and controlled microsolvation conditions. Copyright © 2006 John Wiley & Sons, Ltd.

KEYWORDS: arenium ions; protonated fluorobenzene; electrophilic aromatic substitution; reaction mechanisms; reactive intermediates; IR spectroscopy; photodissociation; structure elucidation

INTRODUCTION

Protonation of aromatic molecules is of central importance to many processes in physical organic chemistry. For example, protonated aromatic molecules (denoted AH^+) appear frequently as short-lived reactive intermediates in fundamental organic reaction mechanisms. One key example is the electrophilic aromatic substitution, the probably most important reaction mechanism of aromatic molecules, in which AH^+ may occur as transient σ complexes (Wheland intermediates) or as π complexes.[1–3] It is well established that fundamental properties of these ionic reactions, such as dynamics and energetics, strongly depend on the solvation environment, mainly because of the significant interaction of the charged reacting species with the surrounding neutral solvent molecules.[1–7] The detailed understanding at the molecular level of the strong impact of solvation on the attributes of the reaction mechanism requires the spectroscopic characterization of AH^+ ions under isolated and controlled microsolvation conditions. In particular, IR spectra of size-selected AH^+–L_m cluster ions are valuable probes of the structure and other relevant properties of AH^+ ions under adjustable solvation conditions by step-wise variation of the number (m) of neutral ligands (L) in the ionic aggregate. However, in contrast to the substantial body of spectroscopic information in the condensed phase (including NMR, IR, and UV spectroscopy as well as X-ray crystallography),[4–13] until recently all experimental data acquired for AH^+ ions isolated in the gas phase came from the radiolytic approach and mass spectrometric techniques.[14–19] Significantly, these techniques provide only indirect and sometimes disputable information about the structure of AH^+ ions. Spectroscopic studies to determine directly and unambiguously, for example, the preferred protonation site in AH^+ ions have been lacking until very recently, mainly due to the difficulties encountered in the production of sufficient AH^+ ion concentrations in the gas phase. However, recent progress in the development of sensitive IR spectroscopic photodissociation schemes, on the basis of the high selectivity of mass spectrometry,[20–26] have allowed for the first time to spectroscopically characterize both isolated (in 2002)[27] and microsolvated (in 2001)[28] AH^+ ions. Meanwhile, there have been a rapidly growing number of studies utilizing either (i) single-photon IR

**Correspondence to:* O. Dopfer, Institut für Atomare Physik und Fachdidaktik, Technische Universität Berlin, Hardenbergstrasse 36, D-10623 Berlin, Germany.
E-mail: dopfer@physik.tu-berlin.de
†Selected paper presented at the 10th European Symposium on Organic Reactivity, 25–30 July 2005, Rome, Italy.

Contract/grant sponsors: Deutsche Forschungsgemeinschaft; Fonds der Chemischen Industrie; European Commission; *Contract/grant numbers:* DO 729; IC 009-04; IC 010-04.

photodissociation (IRPD) of AH^+–L_m clusters[27–37] or (ii) IR multiphoton dissociation (IRMPD) of bare AH^+ ions,[38–42] employing modern optical parametric oscillator (OPO) laser and free electron laser (FEL) systems, respectively. It is the purpose of this review to illustrate the potential of these IR spectroscopic techniques for elucidating subtle details of the structure and chemical reactivity of isolated AH^+ ions free from interference with any solvation effects. IR spectroscopy is an ideal tool to probe, via the measurement of vibrational frequencies, directly the geometrical and energetic parameters of selected chemical bonds in these fundamental reaction intermediates.

The present review is organized as follows. After describing the main experimental strategies for obtaining IR spectra of isolated and microsolvated AH^+ ions, the results will be illustrated in some detail for protonated fluorobenzene as a prototypical AH^+ ion.

EXPERIMENTAL IR(M)PD STRATEGIES

Two major experimental strategies have successfully been employed to obtain IR photodissociation spectra of isolated and microsolvated AH^+ ions. The first technique couples a modern low-intensity OPO laser system, operating in the 2500–4000 cm^{-1} range, with a tandem quadrupole mass spectrometer to record single-photon IRPD spectra of weakly bound AH^+–L_m cluster ions.[26] This approach relies on the evaporation of one or more of the weakly bound solvent molecules (L) upon resonant absorption of a single IR photon:

$$AH^+ - L_m + hv_{IR} \rightarrow AH^+ - L_q + (m-q)L \quad (1)$$

The low intensities of the OPO laser available ($E < 1$ mJ/pulse, $I < 200$ kW/cm^2, $P < 20$ mW) are usually insufficient to drive multiphoton processes.[27,43] The influence of the ligands on the IR spectrum of the central AH^+ ion depends on several factors, including the strength of the interaction, the type of ligand (polar or nonpolar), the site of solvation, and the type of vibration. The effects of microsolvation on the properties of the bare AH^+ ion may be controlled by the systematic variation of L (i.e., the strength of the interaction), the degree of solvation (m), and the comparison with quantum chemical calculations.[32,44–48] In many cases, the perturbation of AH^+ induced by the ligands can be neglected (messenger technique).[30,49] This type of IRPD spectroscopy has so far been applied to AH^+–L_m clusters with aromatic molecules A = benzene,[29–31] (*para*-halogenated) phenols,[28,32–34] fluorobenzene,[35] pyridine,[31] and imidazole.[36] Single-photon IRPD can also be applied to certain isomers of bare AH^+ ions, in case they feature weak chemical bonds:

$$AH^+ + hv_{IR} \rightarrow B^+ + C \quad (2)$$

This variant of IRPD has so far been used to characterize the onium isomers of protonated fluorobenzene (HF elimination of the fluoronium isomer)[27] and protonated *para*-fluorophenol (HF and H_2O elimination of the fluoronium and oxonium isomers, respectively).[37] However, one-photon IRPD usually fails to dissociate common AH^+ ions, because the energy of a single IR photon is insufficient to break strong covalent bonds.[27,35,37]

The shortcut of single-photon IRPD is overcome by the second major experimental strategy, which couples a high-intensity FEL, operating in the 50–2500 cm^{-1} range, with ion cyclotron resonance (ICR) mass spectrometry to drive IR multiphoton photodissociation (IRMPD) of strongly bound AH^+ ions:[50–52]

$$AH^+ + nhv_{IR} \rightarrow B^+ + C \quad (3)$$

The high intensities of the FEL available ($E < 100$ mJ/macropulse, $P < 1$ W) are usually sufficient to drive multiphoton absorption processes. IRMPD spectroscopy has recently been applied to AH^+ ions with A = benzene,[38,39] phenylsilane,[40] benzoic acid,[41] fluorobenzene,[39] and toluene.[42]

As all three processes described in Eqns (1)–(3) have been utilized to characterize various isomers of protonated fluorobenzene,[27,34,35,39] this molecule has been chosen here to illustrate the possibilities of both the IRPD and the IRMPD approaches for spectroscopically characterizing the structure and reactivity of elementary protonated aromatic molecules.

BACKGROUND INFORMATION FOR $C_6H_6F^+$

This section briefly reviews the background information relevant for protonated fluorobenzene ($C_6H_6F^+$).

The potential energy surface (PES) of $C_6H_6F^+$ has been studied in detail by quantum chemical techniques.[27,53–61] Figures 1 and 2 show the minimum structures and the corresponding PES of $C_6H_6F^+$ determined at the B3LYP/6-311G(2df,2pd) level, respectively.[27] Protonation of C_6H_5F can occur at the aromatic ring (**1**–**4**) and at the F atom (**5**), leading to the formation of carbenium and fluoronium ions, respectively. Their relative energies increase in the order **1** < **2** ≪ **3** ≪ **4** ≪ **5**, reflecting the *ortho*/*para* directing nature of the F substituent in electrophilic aromatic substitution reactions. The lowest

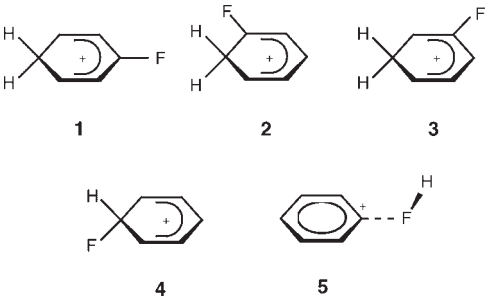

Figure 1. Isomeric structures of protonated fluorobenzene ($C_6H_6F^+$), with protonation occurring at the *para* (**1**), *ortho* (**2**), *meta* (**3**), and *ipso* (**4**) positions as well as at the F atom (**5**)

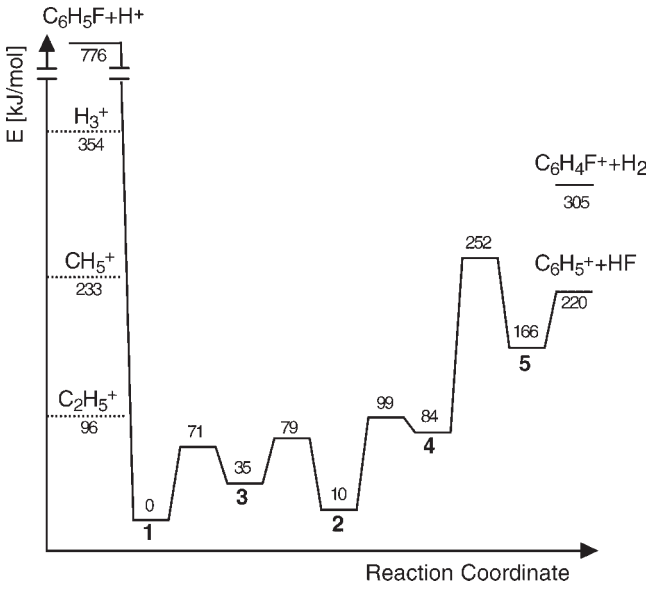

Figure 2. Potential energy surface of $C_6H_6F^+$ calculated at the B3LYP/6-311G(2df,2pd) level.[27] Energies are corrected for zero-point energy. The lowest dissociation channel for all $C_6H_6F^+$ isomers corresponds to fragmentation into $C_6H_5^+$ ($^1A_1$) and HF ($^1\sum^+$). Experimental excess energies for protonation of C_6H_5F in *para* position (**1**) using H_3^+, CH_5^+, and $C_2H_5^+$ are indicated by dotted lines[27,71]

energy interconversion between them proceeds via hydrogen-bridged transition states.[55,62] Isomer **5** is separated from **1**–**4** by a high barrier, whereas the barriers between **1**–**4** are significantly smaller. All minima on the PES correspond to σ complexes and no stable π complex could be located. Protonation at the F substituent considerably destabilizes the strong C—F single bond of C_6H_5F. Hence, **5** is best described as a weakly bound electrostatic ion–dipole complex between the phenyl cation in its singlet ground state and HF, $C_6H_5^+$—FH, with a relatively low dissociation energy of the order of 50 kJ/mol. Consequently, dehydrofluorination is by far the lowest dissociation channel for **1**–**5**, whereas H_2 loss is significantly higher in energy (by about 85 kJ/mol). In addition to **5**, several other less stable ion–dipole complexes of the type $C_6H_5^+$—FH were located on the $C_6H_6F^+$ PES.[27]

Early experimental information about the structure of $C_6H_6F^+$ in the condensed phase was provided by ^{1}H- and ^{19}F-NMR spectroscopy in superacid solutions.[62,63] A static σ complex **1** was identified at low temperature, whereas complete scrambling of all ring protons occurred in the high-temperature limit due to rapid intramolecular 1,2 H-shift. Only the carbenium isomers **1**–**3** could be detected, and no experimental evidence was presented for the existence of a π complex or the fluoronium isomer **5** in these solutions.

As for the gas phase, until recently all experimental information for isolated $C_6H_6F^+$ was provided either from the radiolytic approach[64,65] or from mass spectrometry,[53,55,56,60,61,66–70] including high-pressure mass spectrometry, proton transfer equilibria measurements, metastable decay (MD) analysis, kinetic energy release measurements, and collision-induced dissociation (CID) experiments. The protonation sites inferred for $C_6H_6F^+$, when produced by either chemical ionization (CI) or electron ionization (EI), depended strongly on the ion source conditions, including temperature, pressure, and the protonating agent and precursor employed for the CI and EI processes, respectively. Moreover, both kinetic and thermodynamic factors strongly affect the isomer ratios observed. The experimental proton affinities (PA)[53,71] of C_6H_5F for generating **1** and **5** of 755.9 and 577 ± 24 kJ/mol are in accord with the calculated values of 776 and 610 kJ/mol, respectively (Fig. 2). Although **5** is substantially less stable than **1**–**4**, significant concentrations of **5** can be generated by near resonant proton transfer, that is using a Brønsted acid for protonation with similar or slightly smaller PA, such as CH_5^+ ($PA_{CH_4} = 544$ kJ/mol).[71] Once stable **5** is formed, its conversion into the more stable isomers **1**–**4** is strongly hindered by a high isomerization barrier of the order of 86 kJ/mol. In contrast, **5** cannot be produced in significant abundance using protonating agents with significantly lower or higher PA, such as H_3^+ or $C_2H_5^+$ ($PA_{H_2} =$ 422 kJ/mol, $PA_{C_2H_4} = 681$ kJ/mol).[71] In the first case, the large excess energy involved in the proton transfer step creates internally hot **5**, which results in quantitative unimolecular dissociation via HF loss. In the latter case, the proton transfer reaction generating **5** is endothermic preventing direct protonation at the F atom.

SPECTROSCOPIC RESULTS

This section reviews recent IR spectroscopic studies for $C_6H_6F^+$, which could unambiguously identify the protonation site. (a) First, the single-photon IRPD spectra of bare $C_6H_6F^+$ display the selective detection of isomer **5**, and the analysis of the C—H and C—F stretching frequencies provides spectroscopic confirmation of the HF—$C_6H_5^+$ ion–dipole notation of **5**.[27] Significantly, the IRPD spectrum of **5** was the first IR spectrum recorded for an isolated AH^+ ion. (b) Second, the single-photon IRPD spectrum of $C_6H_6F^+$—$(N_2)_2$ monitored in $C_6H_6F^+$ fragment channel allowed for the selective detection of the most stable carbenium isomers of $C_6H_6F^+$, **1** and **2**.[35] Systematic comparison of their aliphatic C—H stretch frequencies with those of related carbenium ions reveals the effects of the substitution of functional groups on the reactivity of the CH_2 group,[34,35] which corresponds to the reactive center of these arenium ions in, for example, electrophilic aromatic substitution. (c) Finally, the IRMPD spectrum of $C_6H_6F^+$ selectively detected also only the carbenium isomers **1** and **2**, and the comparison of the vibrational spectrum in the fingerprint range (1000–1800 cm^{-1}) with those of C_6H_5F and $C_6H_7^+$ reveals the impact of both protonation and H → F substitution on the structure and reactivity of these aromatic molecules.[39]

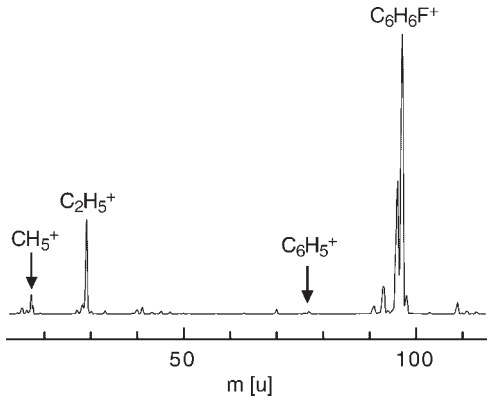

Figure 3. Mass spectrum of the EI ion source for an expansion of C_6H_5F seeded in a CH_4/Ar mixture (1:1 ratio) at 8 bar stagnation pressure.[27] The most intense peaks are assigned to $C_6H_6F^+$, $C_6H_5F^+$, CH_5^+, and $C_2H_5^+$

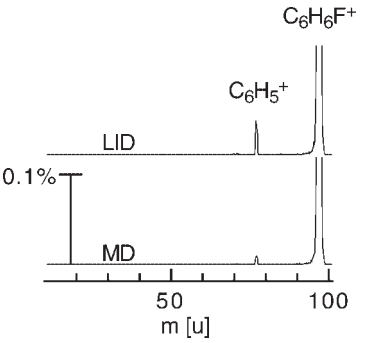

Figure 4. Mass spectra obtained by mass selecting $C_6H_6F^+$ with QMS1 and scanning QMS2 to monitor metastable decay (MD) and laser-induced dissociation (LID, $\nu_{IR} = 3645\,cm^{-1}$).[27] Both processes are dominated by HF loss

IRPD of $C_6H_6F^+$

The relatively low dissociation energy of the fluoronium isomer of $C_6H_6F^+$ (**5**) with respect to dehydrofluorination, $D_0 \sim 50$ kJ/mol (Fig. 2), is of the order of the C—H and F—H stretch frequencies, and thus offers the possibility to selectively detect this particular isomer via resonant single-photon IRPD spectroscopy using a tunable narrow-band OPO laser:[27]

$$C_6H_6F^+ + h\nu_{IR} \rightarrow C_6H_5^+ + HF \qquad (4)$$

To this end, IRPD spectra of $C_6H_6F^+$ were recorded in a tandem quadrupole mass spectrometer (QMS1/2) coupled to an EI ion source and an octopole ion trap. The $C_6H_6F^+$ ions were generated in a high-pressure supersonic plasma expansion, which combines EI with a molecular beam.[27] Figure 3 shows a typical mass spectrum of the EI ion source for an expansion of C_6H_5F seeded in a CH_4/Ar mixture (1:1 ratio) at 8 bar stagnation pressure. The mass spectrum is dominated by $C_6H_6F^+$, $C_6H_5F^+$, CH_5^+, and $C_2H_5^+$. EI of CH_4 and subsequent ion–molecule reactions generate the Brønsted acids CH_5^+ and $C_2H_5^+$, which in turn protonate C_6H_5F via proton transfer. The $C_6H_6F^+$ ions generated were stabilized by collisional cooling in the high-pressure region of the plasma expansion. The presence of CH_5^+ and $C_2H_5^+$ ensured the production of significant concentrations of both carbenium and fluoronium isomers of $C_6H_6F^+$. These were mass selected by QMS1 and the prepared $C_6H_6F^+$ ion beam interacted in an adjacent octopole trap with the OPO laser beam. Resonant excitation of $C_6H_6F^+$ into metastable vibrational levels induced fragmentation into the phenyl cation and HF, which is the lowest energy dissociation channel accessible (Fig. 2, Eqn (4)). No other fragment channel was observed upon single-photon IR excitation. The $C_6H_5^+$ fragment ions were filtered by QMS2 and monitored as a function of the OPO laser frequency (ν_{IR}) to obtain the IRPD spectrum of $C_6H_6F^+$. Figure 4 reproduces mass spectra obtained by selecting $C_6H_6F^+$ with QMS1 and scanning QMS2 to monitor MD and resonant laser-induced dissociation (LID). MD originates from fragmentation of initially hot $C_6H_6F^+$ ions in the octopole (mainly HF loss), which survive the passage through QMS1 as parent ions (≈500 μs). For the LID spectrum, the laser was set resonant to the intense F—H stretch vibration (σ_{FH}) of **5** at 3645 cm^{-1} and additional laser-induced fragmentation into the $C_6H_5^+$ channel was observed. The MD and LID signals in the $C_6H_5^+$ channel correspond to 0.01% and 0.03% of the $C_6H_6F^+$ parent ion signal, respectively. The low MD yield indicates internally cold $C_6H_6F^+$ ions in the octopole, whereas the low LID yield reflects the low photodissociation efficiency of single-photon IRPD.

Figure 5 compares the IRPD spectrum of $C_6H_6F^+$ recorded between 2540 and 4050 cm^{-1} with stick spectra calculated for all possible $C_6H_6F^+$ isomers as well as the planar HF^{mo}—$C_6H_5^+$ ion–dipole complex (≈27 kJ/mol), in which the F atom of HF forms bifurcated H-bonds to the two protons in *meta* and *ortho* position of $C_6H_5^+$ (the most strongly bound isomer of this type of complex).[27] Clearly, the experimental IRPD spectrum is dominated by absorptions of the fluoronium isomer (**5**), whereas absorptions of the more stable carbenium isomers (**1**–**4**) are completely lacking. The analysis of the $C_6H_6F^+$ spectrum spectroscopically confirms the notation of a weakly bound HF—$C_6H_5^+$ ion–dipole complex of **5** predicted theoretically. Indeed, the low dissociation energy of **5** with respect to HF loss is an interesting example of C—F bond destabilization upon protonation. The inert C—F bond in stable fluorocarbons is apparently the strongest single bond that carbon can form.[72] Interestingly, this bond can be significantly weakened and activated by attaching either a proton or a metal cation to the F atom, respectively.[73,74] The IRPD spectrum of **5** provides spectroscopic proof for the protonation-induced C—F bond activation in C_6H_5F. For example, the F—H stretch vibration of **5** ($\sigma_{FH} = 3645\,cm^{-1}$) is much closer to that of

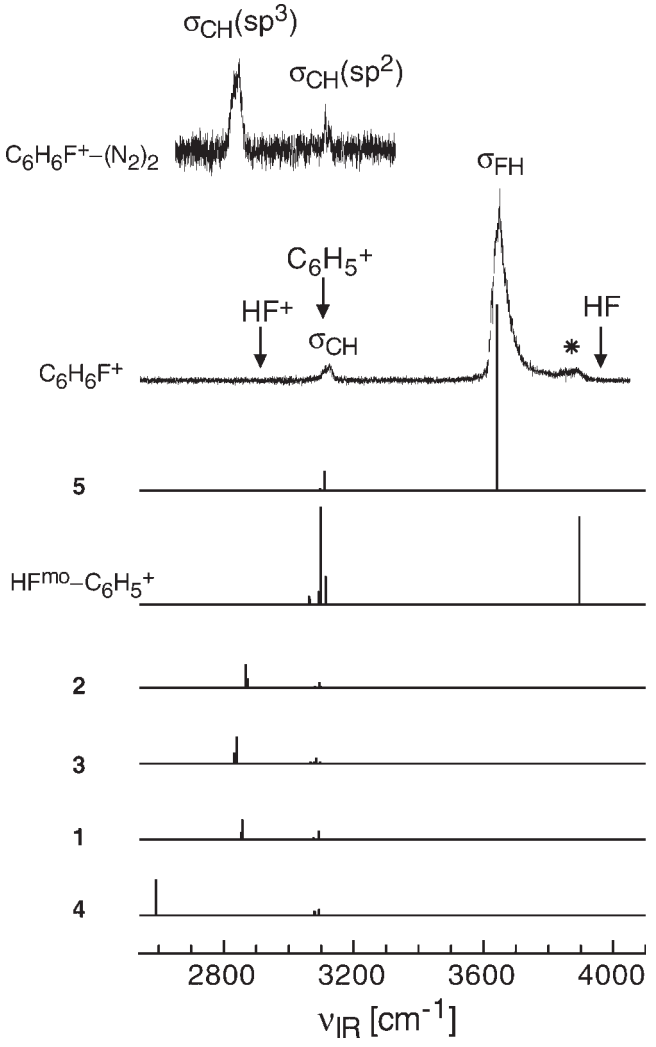

Figure 5. Experimental IRPD spectra of $C_6H_6F^+$ (recorded in the $C_6H_5^+$ channel)[27] and $C_6H_6F^+$–$(N_2)_2$ (recorded in the $C_6H_6F^+$ channel)[35] are compared to stick spectra of the fluoronium isomer of $C_6H_6F^+$ (**5**), the HF^{mo}–$C_6H_5^+$ ion–dipole complex, and the carbenium isomers of $C_6H_6F^+$ (**1**–**4**) calculated at the B3LYP/6-311G(2df,2pd) level (scaling factor 0.96406).[27] The relative intensities in the stick spectra of different isomers reflect directly the calculated IR oscillator strengths. The F–H stretch frequencies of HF and HF^+ at 3961.4 and 2912.5 cm^{-1}, as well as the C–H stretch frequency of $C_6H_5^+$ deposited in argon at 3110 cm^{-1}, are indicated by arrows.[75,76,78] The assignment of the band marked with an asterisk is ambiguous

neutral HF (3961.4 cm^{-1})[75] than to that of the HF^+ cation (2912.5 cm^{-1}),[76] consistent with the modest predicted charge transfer from $C_6H_5^+$ to HF (0.17 e) in HF—$C_6H_5^+$.[27] Similarly, σ_{FH} of **5** is much higher than the average F—H stretch frequency in HFH^+, ν_{av} = 3342.2 cm^{-1},[77] demonstrating the stabilizing effect of charge delocalization in the $C_6H_5^+$ ring on the F—H bond upon substituting H^+ by $C_6H_5^+$. Indeed, $PA_{C_6H_5F}$ for F protonation (577 ± 24 kJ/mol) is much larger than PA_{HF} (484 kJ/mol).[53,71] The second transition observed at 3125 cm^{-1} is assigned to the antisymmetric C—H stretch of the two *ortho* H atoms of **5** (σ_{CH}) and compares favorably with the corresponding transition of bare $C_6H_5^+$ isolated in an Ar matrix (3110 cm^{-1}).[78] In contrast to σ_{FH} and σ_{CH} of **5**, the interpretation of the weak band around 3885 cm^{-1} (marked by an asterisk in Fig. 5) is less certain. Possible assignments include combination bands of **5** (not included in the simulations) or σ_{FH} of less stable HF—$C_6H_5^+$ complexes, such as HF^{mo}—$C_6H_5^+$, which may be created in the employed supersonic plasma expansion. The calculated dissociation energy of **5** for HF loss (D_0 = 4521 cm^{-1}) slightly exceeds the fundamental frequencies of σ_{FH} and σ_{CH}. On the other hand, the linear laser power dependence of the IRPD signals strongly suggests the observation of single-photon absorption processes. Hence, the transitions observed in the IRPD spectrum of **5** must arise from ions containing a certain amount of (ro)vibrational internal energy prior to photoexcitation, that is, they correspond to sequence transitions of the form $\sigma_{CH/FH} + \nu_X \leftarrow \nu_X$, where ν_X are low-frequency inter- and/or intramolecular modes. As a result, the widths of the transitions are relatively broad (30–45 cm^{-1}). Assuming single-photon absorption of relatively cold **5** and a binding energy of $D_0 \approx 4500\ cm^{-1}$, the rovibrational excitation of the $C_6H_5^+$ and HF dissociation products must be small. The HF fragment is in the vibration less $^1\sum^+$ electronic ground state with low rotational excitation. The $C_6H_5^+$ fragment is the phenyl cation in its $^1A_1$ electronic ground state (with probably only minor vibrational excitation), as the lowest triplet state ($^3B_1$) and the most stable acyclic $C_6H_5^+$ isomers are at least ≈0.8–1 eV higher in energy.[70,79] Hence, IRPD of **5** does not induce ring opening, consistent with previous kinetic energy release data.[55,61]

Significantly, the IRPD spectrum of $C_6H_6F^+$ completely lacks contributions of carbenium isomers (**1**–**4**). Their characteristic fingerprint transitions in this spectral range arising from the aliphatic C—H stretch vibration(s) of the (substituted) methylene group near 2600 (**4**) and 2900 cm^{-1} (**1**–**3**) are clearly absent. At first glance, this result may be surprising because the carbenium ions are certainly more stable than **5** and at least the most stable of them (**1**, **2**) certainly occur with significant abundance in the generated $C_6H_6F^+$ ion beam. However, overcoming the barrier for dehydrofluorination of cold carbenium isomers requires at least ≈170 kJ/mol ≈14 200 cm^{-1} (for **4**) corresponding to the absorption of more than four photons with $\nu_{IR} \approx 3000\ cm^{-1}$ (Fig. 2). Apparently, the available OPO laser intensity (200 kW/cm^2) is insufficient to drive this multiphoton process. On the other hand, resonant single-photon dissociation of carbenium ions requires initial internal energies of >130 kJ/mol. Evidently, the population of such energetic carbenium ions in the $C_6H_6F^+$ beam is below the detection limit when CH_5^+/$C_2H_5^+$ is used for protonation. This result is also consistent with the small MD signal in the mass spectra in Fig. 4.

IRPD of $C_6H_6F^+$–L_m

In an effort to spectroscopically detect selectively only carbenium isomers of $C_6H_6F^+$, the IRPD spectrum of $C_6H_6F^+$—$(N_2)_2$ was recorded in the $C_6H_6F^+$ fragment channel using the OPO laser:[35]

$$C_6H_6F^+ - (N_2)_2 + h\nu_{IR} \rightarrow C_6H_6F^+ + 2N_2 \qquad (5)$$

The $C_6H_6F^+$—$(N_2)_2$ spectrum was recorded with the same setup as described above.[26] $C_6H_6F^+$—$(N_2)_2$ cluster ions were generated in a high-pressure supersonic plasma expansion of C_6H_5F seeded at room temperature in a H_2/He/N_2 mixture (1:1:20 ratio) at 8 bar stagnation pressure. EI of this mixture suppressed the production of **5** and generated mainly carbenium isomers of $C_6H_6F^+$. Clusters with N_2 ligands were created by subsequent three-body association reactions in the high-pressure region of the expansion. The $C_6H_6F^+$—$(N_2)_2$ ions were selected by QMS1, interacted in the adjacent octopole with the OPO laser pulse, and the $C_6H_6F^+$ fragment ions produced in reaction (5) were selected by QMS2 and monitored as a function of ν_{IR} to obtain the IRPD spectrum of $C_6H_6F^+$—$(N_2)_2$.

According to IRPD spectra and calculations for the related $C_6H_7^+$—$(N_2)_2$ complex,[29,30] both N_2 ligands in $C_6H_6F^+$—$(N_2)_2$ with carbenium ions form weak intermolecular π bonds to the $C_6H_6F^+$ ring, with dissociation energies of the order of 800 cm^{-1} (≈10 kJ/mol). In contrast, in **5**—$(N_2)_2$ one N_2 ligand is relatively strongly H-bonded to the acidic FH group (with a calculated dissociation energy of ≈57 kJ/mol), whereas the second ligand is probably π-bonded by ≈10 kJ/mol. Hence, whereas the IR photon energy (≈30–40 kJ/mol) is sufficient to evaporate both N_2 ligands of **1**–**4**—$(N_2)_2$, it is not enough to cleave both intermolecular bonds in **5**—$(N_2)_2$. Consequently, the IRPD spectrum of $C_6H_6F^+$—$(N_2)_2$ monitored in the $C_6H_6F^+$ channel should selectively show absorptions of only the **1**–**4**—$(N_2)_2$ isomers. Moreover, as both N_2 ligands are only weakly π-bonded to **1**–**4**, the IRPD spectra of **1**–**4**—$(N_2)_2$ are expected to be very similar to those of bare **1**–**4**.[29,30] The IRPD spectrum of $C_6H_6F^+$—$(N_2)_2$ in Fig. 5 is indeed in close agreement with those calculated for **1**–**3**, confirming the small perturbation by the N_2 ligands. The spectrum is dominated by the symmetric and antisymmetric C—H stretch modes of the aliphatic CH_2 group, $\sigma_{CH}(sp^3)$ ≈2840 cm^{-1}, and weaker absorptions arising from aromatic C—H stretch modes, $\sigma_{CH}(sp^2)$ ≈3125 and 3113 cm^{-1}. The widths of individual bands in the $C_6H_6F^+$—$(N_2)_2$ spectrum (<10 cm^{-1}) are significantly smaller than those of the $C_6H_6F^+$ spectrum (≥30 cm^{-1})[27] because of better effective cooling upon N_2 complexation in the former case.[25,43]

Several plasma-chemical, thermochemical, theoretical, and spectroscopic arguments strongly suggest that the $C_6H_6F^+$—$(N_2)_2$ spectrum in Fig. 5 arises mainly from complexes of **1** and **2**. First, $C_6H_6F^+$ is produced by protonation of C_6H_5F using acids XH^+ in which X has a PA very different from that of C_6H_5F for F protonation (mainly X = He, H_2, and N_2, with PA = 178, 422, and 494 kJ/mol),[71] leading to nearly exclusive production of carbenium isomers. Even if **5**—$(N_2)_2$ were produced in significant abundance, the large total dissociation energy for both ligands (≈67 kJ/mol) prevents the observation of the IRPD process described in Eqn (5). Experience with the generation of related AH^+ ions in the employed ion source[28,32] suggests that the production of **3** and **4** is very inefficient due to low isomerization barriers (35 and 15 kJ/mol) toward the significantly more stable isomers **1** or **2**.[27] Furthermore, the observed relative intensity ratios of the $\sigma_{CH}(sp^3)$ and $\sigma_{CH}(sp^2)$ transitions are in good agreement with those calculated for **1**–**3**, indicating that the $C_6H_6F^+$—$(N_2)_2$ spectrum lacks large contributions from complexes of both **4** and **5**. Moreover, the calculated $\sigma_{CH}(sp^3)$ frequencies of **3** are significantly lower than those for **1** and **2** (by ≥20 cm^{-1}). Hence, as (scaled) calculated frequencies tend to underestimate $\sigma_{CH}(sp^2)$ but overestimate $\sigma_{CH}(sp^3)$,[29,30] comparison with the spectra calculated for **1**–**3** implies only minor contributions of **3** to the $C_6H_6F^+$—$(N_2)_2$ spectrum. In summary, although on the basis of the calculated and experimental spectra in Fig. 5 alone a small contamination of clusters of **3**–**5** to the aromatic C—H stretch bands in the $C_6H_6F^+$—$(N_2)_2$ spectrum cannot be completely ruled out, all arguments strongly suggest clusters of **1** and **2** to be by far the predominant carrier of the observed spectrum.

The frequencies of the C—H stretch vibrations of the aliphatic CH_2 group in substituted arenium ions, $\sigma_{CH}(sp^3)$, are directly correlated to the corresponding C—H bond strengths.[34] Hence, the systematic comparison of $\sigma_{CH}(sp^3)$ of a variety of (poly)substituted AH^+ ions reveals directly the influence of the substitution of functional groups on the intrinsic chemical properties of these important reaction intermediates, because the CH_2 group represents the reactive center of the arenium isomers of AH^+ ions in, for example, electrophilic aromatic substitution reactions.[1,2] Figure 6 compares the IRPD spectra of a variety of (substituted) AH^+–L_m ions (L = Ar or N_2, m = 1 or 2), namely AH^+ = protonated benzene ($C_6H_7^+$, a),[29,30] protonated fluorobenzene ($C_6H_6F^+$, b),[35] protonated phenol ($C_6H_7O^+$, c),[32,33] protonated *para*-fluorophenol ($C_6H_6FO^+$, d),[34] and protonated *para*-chlorophenol ($C_6H_6ClO^+$, e).[34] The spectral range investigated (2700–3000 cm^{-1}) covers the C—H stretch fundamentals of the aliphatic CH_2 group in arenium ions, which typically occur near 2800 cm^{-1}.[5,29] The ligands L act only as a messenger and have virtually no influence on the properties of the aliphatic C—H bonds of the arenium isomers of AH^+ ($\Delta\sigma_{CH}(sp^3) < 3\ cm^{-1}$), because they bind either to the acidic OH group (if present) or to the π electron system.[29,32] Figure 6 compares the IRPD spectra of AH^+–L_m directly to IR spectra calculated for the most stable arenium isomers of the bare AH^+ ions. As expected, the $\sigma_{CH}(sp^3)$ frequencies

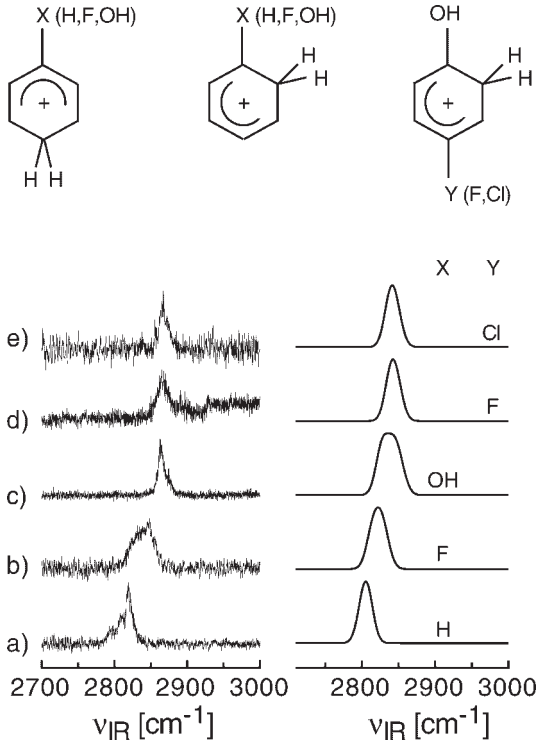

Figure 6. Structures of investigated arenium ions: *para*-protonated $C_6H_6X^+$ (X = H, F, OH), *ortho*-protonated $C_6H_6X^+$ (X = H, F, OH), and *ortho*-protonated $C_6H_6OY^+$ (Y = F, Cl). Experimental IRPD spectra of $C_6H_7^+$–Ar (a),[29] $C_6H_6F^+$–$(N_2)_2$ (b),[35] $C_6H_7O^+$–Ar (c),[32] $C_6H_6OF^+$–Ar (d),[34] and $C_6H_6OCl^+$–Ar (e),[34] recorded in the range of the aliphatic C–H stretch fundamentals, are compared to corresponding IR absorption spectra of $C_6H_7^+$ (a), *p/o*-$C_6H_6F^+$ (b), *p/o*-$C_6H_7O^+$ (c), *o*-$C_6H_6OF^+$ (d), and *o*-$C_6H_6OCl^+$ (e) calculated at the B3LYP/6-311G(2df,2pd) level (convolution width 20 cm^{-1}, scaling factor 0.95)[34]

depend sensitively on the substitution of the functional groups X and Y (Table 1), reflecting directly their influence on the stability of the aliphatic C—H bonds. The higher σ_{CH}, the stronger and shorter are the C—H bonds of the aliphatic CH_2 group. The substantial variation in $\sigma_{CH}(sp^3)$, 2795–2877 cm^{-1}, demonstrates that IR spectroscopy is a sensitive probe for the reactivity of the CH_2 group.

Table 1 compares calculated properties of the aliphatic CH_2 group in the considered arenium ions.[34] The aliphatic C—H bonds in $C_6H_7^+$ are relatively weak, as demonstrated by the comparatively large separation ($R_{CH} = 1.1054$ Å) and low averaged $\sigma_{CH}(sp^3)$ frequencies ($\approx$2804 cm^{-1}). The most stable $C_6H_6F^+$ isomers, *p/o*-$C_6H_6F^+$ (**1/2**), have significantly shorter C—H bonds ($R_{CH} \approx 1.1032$ Å) and correspondingly higher $\sigma_{CH}(sp^3)$ values ($\approx$2822 cm^{-1}) than $C_6H_7^+$. Similar to fluorobenzene, phenol prefers protonation in *para* and *ortho* position (*p/o*-$C_6H_7O^+$), and replacing F by OH strengthens the aliphatic C—H bonds even further ($R_{CH} \leq 1.1010$ Å, $\sigma_{CH} \leq 2838$ cm^{-1}). The preferred protonation site of *para*-halogenated phenols (Y = F, Cl) is in *ortho* position with respect to the OH group (*o*-$C_6H_6FO^+$, *o*-$C_6H_6ClO^+$). According to the calculations, *para*-halogenation of *o*-$C_6H_7O^+$ has only a minor destabilizing effect on the aliphatic C—H bonds ($\Delta R_{CH} \leq 0.0004$ Å, $|\Delta\sigma_{CH}(sp^3)| \leq 5$ cm^{-1}), which are located in *ortho* and *meta* position of the OH and F/Cl substituents, respectively. In general, the predicted substitution effects are nicely confirmed by the IRPD spectra. H → F → OH substitution of benzenium increasingly stabilizes the aliphatic C—H bonds of the most abundant *para*/*ortho*-protonated arenium isomers. In contrast *para*-halogenation of phenol with both F and Cl has virtually no effect on the CH_2 group of the arenium ion, which displays protonation in *ortho* position of the OH group. The first trend is in line with the PA of the substituted aromatic molecules, $PA_{C_6H_6O} > PA_{C_6H_5F} > PA_{C_6H_6}$ (817 > 756 > 750 kJ/mol), consistent with the increasing stabilization of the aliphatic C—H bonds upon H → F → OH substitution. On the other hand, the PA of phenol differs significantly from that of *para*-fluorophenol (817 > 775 kJ/mol), although the $\sigma_{CH}(sp^3)$ frequencies are rather similar. Apparently, the PA provides only a rough indication of the aliphatic C—H bond strength, possibly because the reaction coordinate for proton attachment is slightly different from the C—H stretch normal modes.

Table 1. Calculated properties of the C–H bonds of the aliphatic CH_2 group in selected arenium ions (AH^+, Fig. 6) compared to experimental values.[34]

AH^+ ion	R_{CH} (Å) calc[a]	σ_{CH} (cm^{-1}) calc[a]	σ_{CH} (cm^{-1}) exp
$C_6H_7^+$	1.1054	2801, 2807	2795, 2810
p-$C_6H_6F^+$ (**1**)	1.1038	2813, 2816	2840[b]
o-$C_6H_6F^+$ (**2**)	1.1026	2826, 2832	2840[b]
p-$C_6H_7O^+$	1.1019	2828, 2829	2864, 2877[b]
o-$C_6H_7O^+$	1.1001	2843, 2853	2864, 2877[b]
o-$C_6H_6OF^+$	1.1004	2840, 2849	2866
o-$C_6H_6OCl^+$	1.1005	2839, 2848	2866

[a] B3LYP/6-311G(2df,2pd) level (scaling factor 0.95).
[b] A specific assignment to either the *ortho* or the *para* isomer is impossible at the present stage. Probably both isomers contribute to the experimental IR signal.

IRMPD of $C_6H_6F^+$

In order to detect the IR spectrum of possible carbenium and fluoronium isomers of bare $C_6H_6F^+$ in the frequency range below 2500 cm^{-1}, IRMPD spectra of $C_6H_6F^+$ were recorded in an FT-ICR mass spectrometer utilizing the FEL at CLIO (*Centre Laser Infrarouge Orsay*). This effort extended the previous spectroscopic interrogations of $C_6H_6F^+$ using the OPO laser in various aspects.[27,34,35] First, the spectral range covered using the FEL (600–1700 cm^{-1}) is complementary to that using the OPO (2540–4050 cm^{-1}), yielding valuable new information on vibrational frequencies in the so-called

fingerprint range. In particular, comparison with the corresponding spectra of C_6H_5F[80] and $C_6H_7^+$[38,39] provided insight into the effects of both protonation and $H \rightarrow F$ substitution on the structural properties of the molecule. Second, the much higher intensity of the FEL ($\sim$1 W) compared to the OPO (<20 mW) opened the possibility to drive multiphoton absorption processes. Hence, in contrast to the OPO studies, all $C_6H_6F^+$ isomers produced could be detected by monitoring IRMPD. Third, whereas most previous studies employed high-pressure ion sources for $C_6H_6F^+$ generation, the ions were created in a low-pressure ICR cell ($5 \times 10^{-9} - 5 \times 10^{-8}$ mbar) via CI using mass-selected CH_5^+ or $C_2H_5^+$ ions. This is an important aspect, as the ion source conditions are crucial for the produced $C_6H_6F^+$ isomer ratio. In addition to the protonation site and its spectroscopic consequences, the differences in the fragmentation branching ratios observed for collisional and infrared activation (CID *vs.* IRMPD) were also addressed.

The experimental setup couples a mobile FT-ICR mass spectrometer analyzer (MICRA) with tunable FEL radiation. Details of the coupling of MICRA[81] with the FEL[82] are described elsewhere.[50,51] The $C_6H_6F^+$ ions were generated in the ICR cell by CI of C_6H_5F using mass-selected CH_5^+ or $C_2H_5^+$ ions. The $C_6H_6F^+$ ions generated were mass selected and subsequently irradiated for 1 s with FEL radiation ($\sim$1 W), which is composed of 8 μs macropulses (25 Hz), each divided into 500 micropulses (few ps long, 16 ns apart). Finally, a mass spectrum was recorded at each frequency of the IR laser to collect the parent and daughter ions, which arise from either IRMPD or unimolecular dissociation. At the employed experimental conditions, LID of $C_6H_6F^+$ occurred predominantly into the lowest-energy fragment channel (96%, HF loss), but loss of H_2 was also observed as a minor fragment channel (4%):

$$C_6H_6F^+ + nh\nu_{IR} \rightarrow C_6H_5^+ + HF \quad (6a)$$

$$C_6H_6F^+ + nh\nu_{IR} \rightarrow C_6H_4F^+ + H_2 \quad (6b)$$

Figure 7 compares the $C_6H_6F^+$ parent ion signal with that of the strongest fragment ion signal ($C_6H_5^+$) as a function of ν_{IR}.[39] Clearly, there is a 1:1 correspondence between the $C_6H_6F^+$ depletion and $C_6H_5^+$ appearance signals with respect to both the positions and the widths of the resonances. For the strongest resonance at 1451 cm^{-1}, the depletion is as large as 40%, indicative of the high efficiency of the IRMPD process. This is in stark contrast to the low efficiency of single-photon IRPD of isomer **5** of $C_6H_6F^+$ illustrated in Fig. 4 (0.03%) for vibrational resonances with comparable IR oscillator strengths, demonstrating the strong dependence of fragmentation yields on the employed IR laser intensity. As the spectra monitored in both channels (6a,b) were similar, only those recorded in the HF loss channel are shown. In current models to describe the IRMPD process, sequential heating of the parent ion occurs via the successive

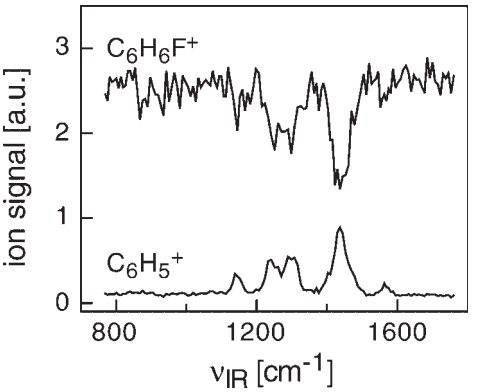

Figure 7. $C_6H_6F^+$ parent ion and $C_6H_5^+$ fragment ion signals (arb. units) as a function of the FEL frequency[39]

absorption of single IR photons intermediated by intramolecular vibrational relaxation. This relatively slow heating process favors dissociation into the lowest energy fragment channel with branching ratios independent of the laser frequency.[83] According to the dissociation energies given in Fig. 2, HF (H_2) loss for cold **1** requires the absorption of $n = 13$ ($n = 18$) photons with $\nu_{IR} = 1450\ cm^{-1}$, respectively. Similarly to IRMPD, both CID experiments of ring-protonated $C_6H_6F^+$ (**1**, **2**) at low collision energies and unimolecular dissociation favor HF over H_2 elimination.[55,61,68] On the other hand, CID at high collision energies induces preferentially H_2 loss rather than HF loss.[56,60,69] Hence, high excitation of **1** and **2** via a single excitation event leads to direct ejection of H_2, which is fast on the timescale required for isomerization via the high barrier toward HF elimination (Fig. 2). In contrast, heating of **1** and **2** in the IRMPD process via the sequential absorption of multiple IR photons appears to be slow enough to facilitate isomerization and subsequent fragmentation into the lowest-energy fragmentation channel. Figure 7 displays significant frequency-independent background signal in the $C_6H_5^+$ channel (4% of parent ions). This background is large only when CH_5^+ is used for $C_6H_6F^+$ generation and is ascribed to MD of hot $C_6H_6F^+$ ions, which is fast ($\tau \sim 10^{-5}$ s)[61] on the timescale of the present experiment ($\sim$1 s).

Figure 8 compares the IRMPD spectrum of $C_6H_6F^+$ to linear IR absorption spectra calculated for the isomers **1**–**5**.[39] No difference was found between the IRMPD spectra of $C_6H_6F^+$ generated with either $C_2H_5^+$ or CH_5^+. Hence, only the one using CH_5^+ is presented in Fig. 8. First, the isomer assignments are considered. Inspection of Fig. 8 immediately reveals convincing agreement between the IRMPD spectrum and the spectra predicted for **1** and **2**. Both isomers are by far the most stable minima on the $C_6H_6F^+$ PES and therefore expected to be generated in significant abundances. In contrast, the IR spectra of **3**–**5** differ qualitatively from the IRMPD spectrum, as is evidenced by the lack of the intense theoretical transitions (indicated by filled circles in Fig. 8)

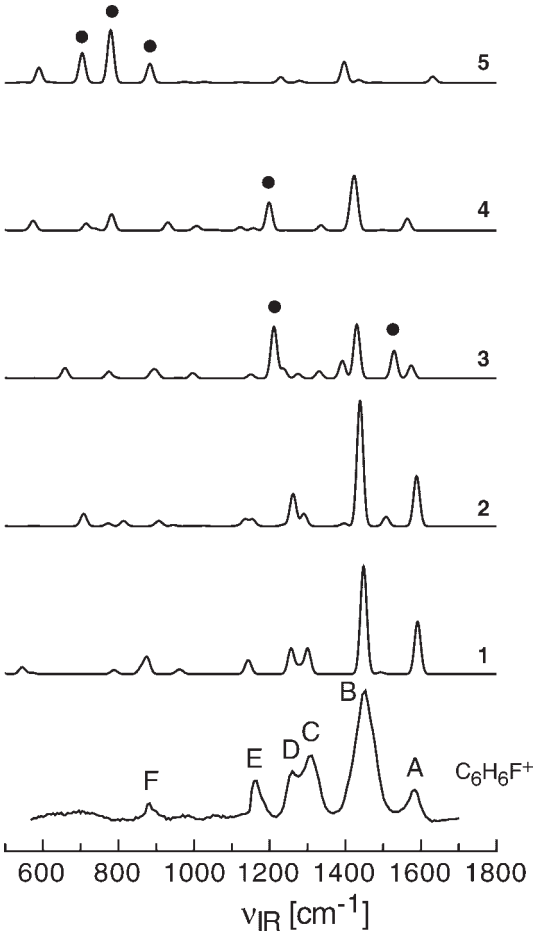

Figure 8. Comparison of the experimental IRMPD spectrum of $C_6H_6F^+$ (using CH_5^+ as protonating agent) monitored in the HF loss channel with linear IR absorption spectra of the isomers **1**–**5** calculated at the B3LYP/6-311G(2df,2pd) level (convolution width 20 cm^{-1}, scaling factor of 0.96).[39] The lack of detection of the intense bands predicted for **3**–**5** (indicated by filled circles) in the measured spectrum strongly suggests that mainly isomers **1** and/or **2** contribute to the experimental spectrum

in the experimental spectrum. Hence, the abundances of **3**–**5** are concluded to be below the detection limit. The absence (or low concentration) of **3** and **4** in the ion source may be rationalized by (i) their smaller stabilization energies compared to **1** and **2** and (ii) their low isomerization barriers toward **1** and/or **2** (Fig. 2). The absence of **5** in the IRMPD spectra when using $C_2H_5^+$ for $C_6H_6F^+$ production is expected, because the $PA_{C_6H_5F}$ for F protonation is smaller than $PA_{C_2H_4}$ (Fig. 2), preventing efficient generation of **5**. The lack of detection of **5** in IRMPD spectra when using CH_5^+ for $C_6H_6F^+$ production may, at first glance, be somewhat surprising because this isomer was previously produced in significant abundance in high-pressure CI ion sources using this Brønsted acid. However, efforts in creating substantial amounts of **5** in the low-pressure ICR cell using CH_5^+ failed, because the low pressure prevents efficient cooling of **5** via three-body collisions. Most of **5** produced in the early stage of the ion–molecule reaction sequence probably decays via MD before interacting with the IR irradiation, giving rise to the constant background in the HF loss channel (Fig. 7).

After assigning the transitions A–F observed in the IRMPD spectrum of $C_6H_6F^+$ to the isomers **1** and/or **2**, their vibrational interpretation is considered.[39] The high-frequency transitions A and B at 1583 and 1451 cm^{-1} are attributed to C—C stretch vibrations, σ_{CC}. Band C at 1308 cm^{-1} corresponds to the C—F stretch mode, σ_{CF}, whereas band D at 1260 cm^{-1} arises from the scissoring motion of the methylene group, β_{CH_2}. Band E at 1161 cm^{-1} can be assigned to in-plane C—H bending motions, β_{CH}, whereas band F at 881 cm^{-1} mainly arises from an out-of-plane ring deformation.

In an effort to unravel the effects of both protonation and H → F substitution, Fig. 9 compares the structural parameters of C_6H_5F, isomer **1** of $C_6H_6F^+$, and $C_6H_7^+$.[39] Major effects of (*para*-)protonation on C_6H_5F include a contraction of the C—F bond ($\Delta R = -0.049$ Å), a deformation of the aromatic ring toward a 1,4-cyclohexadienyl-type structure, and an elongation of the C—H bond at the protonation site ($\Delta R = 0.023$ Å). The excess charge of the attached proton in **1** is largely delocalized over the whole molecule. The six protons carry around 70% of the positive charge ($q_H \sim 0.12$ e), whereas the C atoms and the CF group are less charged (~ 0.05 e). Comparison between $C_6H_7^+$ and **1** demonstrates that H → F substitution slightly enhances the deformation of the aromatic ring induced by protonation. In general, the

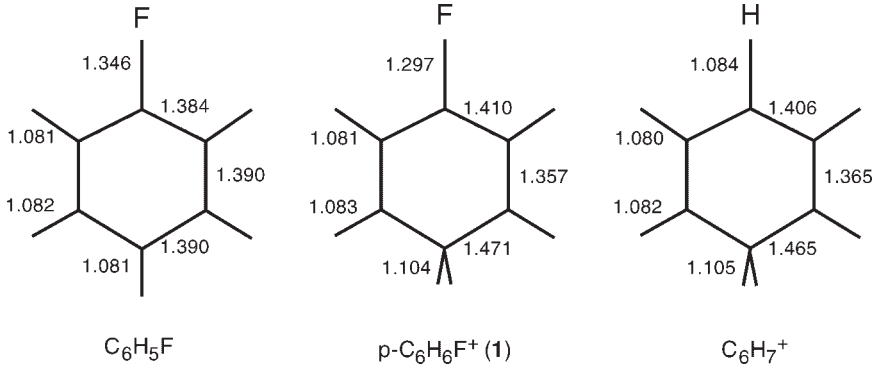

Figure 9. Structural parameters (in Å) of C_6H_5F, $C_6H_6F^+$ (isomer **1**), and $C_6H_7^+$ evaluated at the B3LYP/6-311G(2df,2pd) level[39]

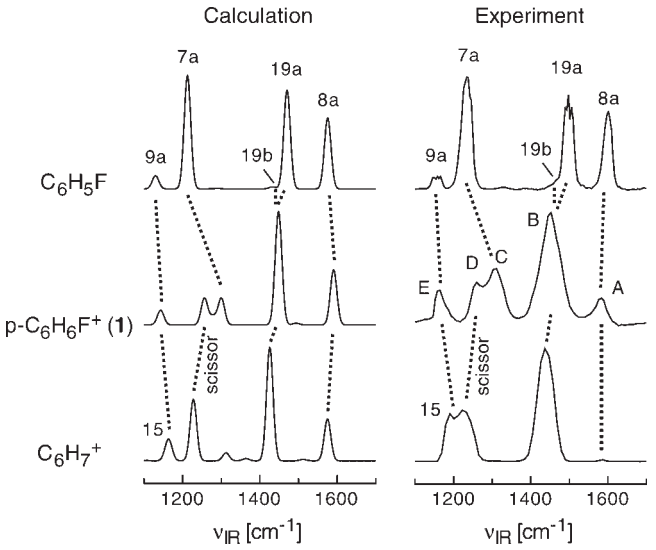

Figure 10. Comparison of linear IR absorption spectra of C_6H_5F, $C_6H_6F^+$ (isomer **1**), and $C_6H_7^+$ calculated at the B3LYP/6-311G(2df,2pd) level (convolution width 20 cm^{-1}, scaling factor 0.96)[39] with the corresponding experimental IR absorption spectrum of C_6H_5F[80] and IRMPD spectra of $C_6H_6F^+$ and $C_6H_7^+$[39]

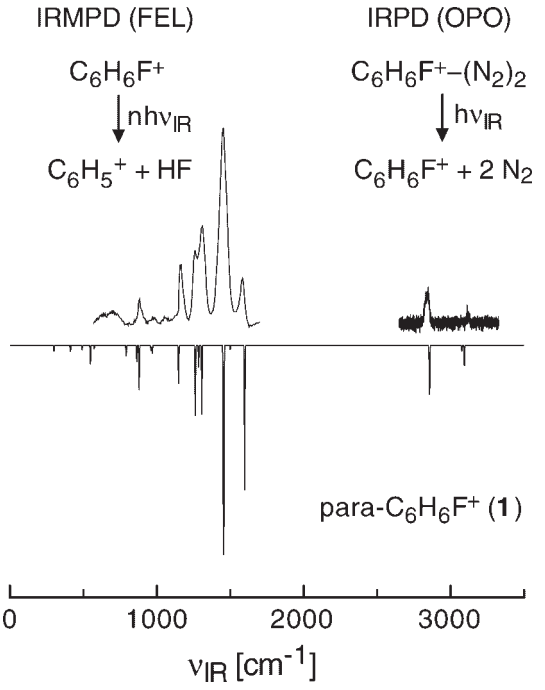

Figure 11. Experimental IR(M)PD spectra of $C_6H_6F^+$ and $C_6H_6F^+$–$(N_2)_2$ (Figs. 5 and 8) compared to a linear IR absorption spectrum of isomer **1** of $C_6H_6F^+$ calculated at the B3LYP/6-311G(2df,2pd) level (convolution width 5 cm^{-1}, scaling factor 0.96406)[39]

arenium ions are best described as (substituted) pentadienyl cations bridged by a methylene group.[54]

The structural implications upon ring protonation and H → F substitution directly transfer into the corresponding IR spectra.[39] Experimental IR spectra of C_6H_5F,[80,84,85] $C_6H_6F^+$, and $C_6H_7^+$,[39] in the fingerprint region are compared in Fig. 10, along with calculated linear IR absorption spectra (**1** is selected for $C_6H_6F^+$). In agreement with the predicted trend, the frequency of the in-plane bend, ν_{9a}, increases in the order $C_6H_5F \rightarrow \mathbf{1} \rightarrow C_6H_7^+$. The contraction of the C—F bond upon *para*-protonation of C_6H_5F results in a significant increase in the C—F stretch frequency, ν_{7a}, from 1239 to 1308 cm^{-1}. In line with the predictions, the frequency of the scissoring mode of the aliphatic CH_2 group in the arenium ions increases substantially upon H → F substitution from 1225 to 1260 cm^{-1}. According to the calculations, *para*-protonation of C_6H_5F nearly removes the splitting between the two C—C stretch modes ν_{19a} and ν_{19b}, leads to an IR enhancement of the weaker ν_{19b} component, and keeps the average frequency of the ν_{19} doublet roughly constant. This trend appears to be confirmed by the experimental IR spectra when taking into account that the blue part of the broad $\nu_{19a/b}$ band (band B) in the experimental $C_6H_6F^+$ spectrum arises from isomer **1**. The red part of band B at 1451 cm^{-1} is ascribed to the corresponding contribution of isomer **2** with slightly lower frequency. Both the calculations and the experimental spectra reveal that H → F substitution slightly increases the frequency of $\nu_{19a/b}$. The highest frequency C—C stretch modes in these simple benzene derivatives correspond to the $\nu_{8a/b}$ doublet, of which only the ν_{8a} component has significant IR intensity. Interestingly, this is the only vibration in this spectral range, for which the predicted protonation effect on the frequency is opposite to the observed trend. In addition, also the relative IR intensity of this band is significantly lower in the IRMPD spectrum. Both effects are attributed to the details of the IRMPD process, which results in an underestimated frequency and IR intensity compared to the predicted linear IR absorption spectrum.[38,39]

The experimental IRMPD and IRPD spectra of $C_6H_6F^+$ and $C_6H_6F^+$—$(N_2)_2$ obtained using the FEL and OPO (taken from Figs. 5 and 8), respectively, are combined in one trace in Fig. 11 and compared to the linear IR absorption spectrum calculated for isomer **1** of $C_6H_6F^+$. As discussed above, the experimental spectra arise mainly from the isomers **1** and **2** of $C_6H_6F^+$, featuring similar IR spectra. Inspection of Fig. 11 reveals (i) good agreement between experiment and theory and (ii) nearly complete coverage of the full IR spectrum of the most stable carbenium isomers of $C_6H_6F^+$ in the spectral range of fundamental frequencies by combining the spectroscopically complementary approaches of IRMPD (FEL) and IRPD (OPO).

CONCLUDING REMARKS AND OUTLOOK

Recent advances in the spectroscopic investigation of protonated aromatic molecules under controlled microsolvation conditions have been reviewed. The spectro-

scopic progress has been made possible by combining the high selectivity of mass spectrometry with the high sensitivity of action spectroscopy using modern IR laser sources, such as FEL and OPO lasers. In particular IR spectroscopy, in combination with quantum chemistry, has proven to be a powerful and promising tool to probe the structure and bonding of AH^+ ions. The application of sensitive IR(M)PD techniques to isolated and microsolvated AH^+ ions have allowed for the first time to spectroscopically characterize the structure and reactivity of these fundamental reaction intermediates, free from interference with any solvation effects. In contrast to the vast body of mass spectrometric data available for AH^+ ions in the literature, the new spectroscopic approaches provide for the first time unambiguous structure determination of bare AH^+ ions, in particular about the preferred site of protonation. Moreover, analysis of the vibrational frequencies yields experimental insight with unprecedented precision into the subtle effects of substitution of functional groups on the chemical reactivity of these fundamental reactive intermediates under isolated and controlled microsolvation conditions.

Future developments will involve the application of these established IR techniques to so far uncharacterized AH^+–L_m cluster ions. One direction is toward larger cluster sizes (m)[33] and toward chemically more relevant solvent molecules (such as water),[25,30,86] in order to establish the link between gas-phase chemistry and chemistry in the condensed phase at the molecular level. Another route is toward larger and more complicated AH^+ ions, such as (microhydrated) protonated biomolecular building blocks. Initial IR studies on microhydrated protonated imidazole,[36] protonated DNA bases, amino acids, and their oligomers,[87–89] have already proven the feasibility of such investigations. In particular, matrix-assisted laser desorption ionization (MALDI)[89] and electrospray ionization (ESI)[87,88] techniques have successfully been used in IR(M)PD studies for creating AH^+ ions from nonvolatile precursors. Finally, extending the spectral range from the IR toward the UV-VIS region, will open the possibility to probe the electronic structure, the excited state dynamics, and photochemical stability of these important (bio)chemical species in more detail.[90–92]

Acknowledgements

The studies in Würzburg and Basel using the OPO laser were parts of the projects DO 729/2 (DFG) and 20-63459.00 (SNF). The studies in Orsay using the FEL at the CLIO facility were supported by the CNRS, the University of Paris-Sud, the MIUR, and the DFG (DO 729/2). Financial support by the European Commission (projects IC 009-04 and IC 010-04) is gratefully acknowledged. O.D. is supported by a Heisenberg Fellowship (DO 729/1) and the *Fonds der Chemischen Industrie*. The author thanks Helmut Schwarz and Detlef Schröder (TU Berlin) for stimulating discussions about the ion–molecule reaction chemistry of $C_6H_6F^+$.

REFERENCES

1. Carey FA, Sundberg RJ. *Advanced Organic Chemistry.* Plenum Press: New York, 1995.
2. Smith MB, March J. *Advanced Organic Chemistry: Reactions, Mechanisms, and Structure*, 5 ed. Wiley: New York, 2001.
3. Lenoir D. *Angew. Chem. Int. Ed*. 2003; **42**: 854.
4. Olah GA, White AM, O'Brien DH. *Chem. Rev.* 1970; **70**: 561.
5. Koptyug VA. *Top. Curr. Chem*. 1984; **122**: 1.
6. Brouwer DM, Mackor EL, MacLean C. Arenonium Ions. In *Carbonium Ions*, vol. II, Olah GA, Schleyer PvR (eds). Wiley: New York, 1970.
7. Perkampus HH, Baumgarten E. *Angew. Chem. Int. Ed. Engl*. 1964; **3**: 776.
8. Hubig SM, Kochi JK. *J. Org. Chem*. 2000; **65**: 6807.
9. Olah GA, Staral JS, Asencio G, Liang G, Forsyth DA, Mateescu GD. *J. Am. Chem. Soc*. 1978; **100**: 6299.
10. Xu T, Barich DH, Torres PD, Haw JF. *J. Am. Chem. Soc*. 1997; **119**: 406.
11. Reed CA, Fackler NLP, Kim KC, Stasko D, Evans DR, Boyd PDW, Rickard CEF. *J. Am. Chem. Soc*. 1999; **121**: 6314.
12. Stasko D, Reed CA. *J. Am. Chem. Soc*. 2001; **124**: 1148.
13. Dewey TX, Barich H, Torres PD, Haw JF. *J. Am. Chem. Soc*. 1997; **119**: 406.
14. Speranza M. *Mass. Spectrom. Rev.* 1992; **11**: 73.
15. Fornarini S. *Mass Spectrom. Rev*. 1996; **15**: 365.
16. Fornarini S, Crestoni ME. *Acc. Chem. Res*. 1998; **31**: 827.
17. Kuck D. *Mass Spectrom. Rev.* 1990; **9**: 583.
18. Chiavarino B, Crestoni ME, Fornarini S. *J. Phys. Org. Chem*. 2004; **17**: 957.
19. Esteves PM, de M, Carneiro JW, Cardoso SP, Barbosa AGH, Laali KK, Rasul G, Prakash GKS, Olah GA. *J. Am. Chem. Soc*. 2003; **125**: 4836.
20. Okumura M, Yeh LI, Lee YT. *J. Chem. Phys*. 1985; **83**: 3705.
21. Duncan MA. *Int. J. Mass Spectrom*. 2000; **200**: 545.
22. Duncan MA. *Int. Rev. Phys. Chem*. 2003; **22**: 407.
23. Robertson WH, Johnson MA. *Annu. Rev. Phys. Chem*. 2003; **54**: 173.
24. Bieske EJ, Dopfer O. *Chem. Rev.* 2000; **100**: 3963.
25. Dopfer O. *Z. Phys. Chem*. 2005; **219**: 125.
26. Dopfer O. *Int. Rev. Phys. Chem*. 2003; **22**: 437.
27. Solcà N, Dopfer O. *J. Am. Chem. Soc*. 2003; **125**: 1421.
28. Solcà N, Dopfer O. *Chem. Phys. Lett*. 2001; **342**: 191.
29. Solcà N, Dopfer O. *Angew. Chem. Int. Ed*. 2002; **41**: 3628.
30. Solcà N, Dopfer O. *Chem. Eur. J*. 2003; **9**: 3154.
31. Chaudhuri C, Wu C-C, Jiang J-C, Chang H-C. *Aus. J. Chem*. 2004; **57**: 1153.
32. Solcà N, Dopfer O. *J. Am. Chem. Soc*. 2004; **126**: 1716.
33. Solcà N, Dopfer O. *J. Chem. Phys*. 2004; **120**: 10470.
34. Solcà N, Dopfer O. *Chem. Phys. Chem*. 2005; **6**: 434.
35. Solcà N, Dopfer O. *Angew. Chem. Int. Ed*. 2003; **42**: 1537.
36. Andrei HS, Solcà N, Dopfer O. *Chem. Phys. Chem*. 2006; **7**: 107.
37. Solcà N, Dopfer O. *J. Chem. Phys*. 2004; **121**: 769.
38. Jones W, Boissel P, Chiavarino B, Crestoni ME, Fornarini S, Lemaire J, Maitre P. *Angew. Chem. Int. Ed*. 2003; **42**: 2057.
39. Dopfer O, Solcà N, Lemaire J, Maitre P, Crestoni ME, Fornarini S. *J. Phys. Chem. A* 2005; **109**: 7881.
40. Chiavarino B, Crestoni ME, Fornarini S, Lemaire J, MacAleese L, Maitre P. *Chem. Phys. Chem*. 2005; **6**: 437.
41. Oomens J, von Helden G, Meijer G. *J. Phys. Chem. A* 2004; **108**: 8273.
42. Dopfer O, Lemaire J, Maitre P, Crestoni ME, Fornarini S. *Int. J. Mass Spectrom*. 2006; **249–250**: 149.
43. Solcà N, Dopfer O. *Chem. Phys. Lett*. 2001; **347**: 59.
44. Olkhov RV, Dopfer O. *Chem. Phys. Lett*. 1999; **314**: 215.
45. Solcà N, Dopfer O. *J. Phys. Chem. A* 2001; **105**: 5637.
46. Dopfer O, Roth D, Maier JP. *Int. J. Mass. Spectr*. 2002; **218**: 281.
47. Dopfer O. *J. Phys. Chem. A* 2000; **104**: 11693.

48. Dopfer O, Roth D, Maier JP. *J. Phys. Chem. A* 2000; **104**: 11702.
49. Dopfer O, Olkhov RV, Maier JP. *J. Chem. Phys*. 1999; **111**: 10754.
50. Maitre P, Le Caer S, Simon A, Jones W, Lemaire J, Mestdagh H, Heninger M, Mauclaire G, Boissel P, Prazeres R, Glotin F, Ortega JM. *Nucl. Instrum. Methods, Sect A* 2003; **507**: 541.
51. Lemaire J, Boissel P, Heninger M, Mauclaire G, Bellec G, Mestdagh H, Simon A, Le Caer S, Ortega JM, Glotin F, Maitre P. *Phys. Rev. Lett*. 2002; **89**: 273002.
52. Valle JJ, Eyler JR, Oomens J, Moore DT, van der Meer AFG, von Helden G, Meijer G, Hendrickson CL, Marshall AG, Blakney GT. *Rev. Sci. Instrum*. 2005; **76**: 023103.
53. Mason R, Milton D, Harris F. *J. Chem. Soc., Chem. Commun*. 1987; 1453.
54. Bader RFW, Chang C. *J. Phys. Chem*. 1989; **93**: 5095.
55. Hrusak J, Schröder D, Weiske T, Schwarz H. *J. Am. Chem. Soc*. 1993; **115**: 2015.
56. Mason RS, Parry AJ, Milton DMP. *J. Chem. Soc. Faraday Trans*. 1994; **90**: 1373.
57. Maksic TB, Kovacevic B, Kovacek D. *J. Phys. Chem. A* 1997; **101**: 7446.
58. Szulejko JE, Hrusak J, McMahon TB. *J. Mass. Spectrom*. 1997; **32**: 494.
59. Wiberg KB, Rablen PR. *J. Org. Chem*. 1998; **63**: 3722.
60. Mason RS, Anderson PDJ, Williams CM. *J. Chem. Soc. Faraday Trans*. 1998; **94**: 2549.
61. Schröder D, Oref I, Hrusak J, Weiske T, Nikitin EE, Zummack W, Schwarz H. *J. Phys. Chem. A* 1999; **103**: 4609.
62. Olah GA, Mo YK. *J. Org. Chem*. 1973; **38**: 3212.
63. Olah GA, Kiovsky TE. *J. Am. Chem. Soc*. 1967; **89**: 5692.
64. Speranza M, Cacace F. *J. Am. Chem. Soc*. 1977; **99**: 3051.
65. Cacace F, Speranza M. *J. Am. Chem. Soc*. 1976; **98**: 7299.
66. Lau YK, Kebarle P. *J. Am. Chem. Soc*. 1976; **98**: 7452.
67. Speranza M, Sefcik MD, Henis JMS, Gaspar PP. *J. Am. Chem. Soc*. 1977; **99**: 5583.
68. Tkaczyk M, Harrison AG. *Int. J. Mass Spectrom. Ion Proc*. 1990; **100**: 133.
69. Tkaczyk M, Harrison AG. *Int. J. Mass Spectrom. Ion Proc*. 1994; **132**: 73.
70. Lorquet JC, Lorquet AJ. *J. Phys. Chem. A* 2001; **105**: 3719.
71. Hunter EPL, Lias SG. *J. Phys. Chem. Ref. Data* 1998; **27**: 413.
72. Hudlicky M. *Chemistry of Organic Fluorine Compounds*. Prentice-Hall: New York, 1992.
73. Plenio H. *Chem. Rev.* 1997; **97**: 3363.
74. Mazurek U, Schwarz H. *Chem. Commun*. 2003; 1321.
75. Le Blanc RB, White JB, Bernath PF. *J. Mol. Spec*. 1994; **164**: 574.
76. Hovde DC, Keim ER, Saykally R. *J. Mol. Phys*. 1989; **68**: 599.
77. Schäfer E, Saykally RJ. *J. Chem. Phys*. 1984; **81**: 4189.
78. Winkler M, Sander W. *Angew. Chem. Int. Ed*. 2000; **39**: 2014.
79. Hrusak J, Schröder D, Iwata S. *J. Chem. Phys*. 1997; **106**: 7541.
80. NIST, Linstrom PJ, Mallard WG. *NIST Chemistry WebBook*; NIST Standards and Technology, Gaithersburg MD, 20899 (http://webbook.nist.gov), 2001.
81. Mauclaire G, Lemaire J, Boissel P, Bellec G, Heninger M. *Eur. J. Mass Spectrom*. 2004; **1**: 155.
82. Prazeres R, Glotin F, Insa C, Jaroszynski DA, Ortega JM. *Eur. Phys. J. D* 1998; **3**: 87.
83. Ervin KM. *Chem. Rev.* 2001; **101**: 391.
84. Varsanyi G. *Assignments for Vibrational Spectra of Seven Hundred Benzene Derivatives*, vol. 1. Wiley: New York, 1974.
85. Lipp ED, Seliskar CJ. *J. Mol. Spec*. 1981; **87**: 255.
86. Solcà N, Dopfer O. *J. Phys. Chem. A* 2003; **107**: 4046.
87. Kamariotis A, Boyarkin OV, Mercier S, Bush MF, Williams ER, Beck RD, Rizzo TR. *J. Am. Chem. Soc*. 2006; **128**: 905.
88. Oh H-B, Lin C, Hwang HY, Zhai H, Breuker K, Zabrouskov V, Carpenter BK, McLafferty FW. *J. Am. Chem. Soc*. 2005; **127**: 4076.
89. Lucas B, Gregoire G, Lemaire J, Maitre P, Glotin F, Scherman JP, Desfracois C. *Int. J. Mass Spectrom*. 2005; **243**: 105.
90. Freiser BS, Beauchamp JL. *J. Am. Chem. Soc*. 1977; **99**: 3214.
91. Marian C, Nolting D, Weinkauf R. *Phys. Chem. Chem. Phys*. 2005; **7**: 3306.
92. Kang H, Jouvet C, Dedonder-Lardeux C, Martrenchard S, Gregoire G, Desfrancois C, Schermann JP, Barat M, Fayeton JA. *Phys. Chem. Chem. Phys*. 2005; **7**: 394.